applied sciences

MDPI

Article

Broadband Dielectric Characterization of High-Permittivity Rogers Substrates via Terahertz Time-Domain Spectroscopy in Reflection Mode

Walter Fuscaldo, Francesco Maita, Luca Maiolo, Romeo Beccherelli and Dimitrios C. Zografopoulos *

Consiglio Nazionale delle Ricerche, Istituto per la Microelettronica e Microsistemi, 00133 Rome, Italy
* Correspondence: dimitrios.zografopoulos@cnr.it

Abstract: We report the dielectric characterization of three commercially available, high-permittivity Rogers laminates in the sub-terahertz range, by means of terahertz time-domain spectroscopy measurements in reflection mode. A transmission-line model is developed to obtain the reflectance spectra as a function of the frequency-dispersive complex relative permittivity of the substrates. The latter is fitted through optimization to a single Lorentzian term, which is shown to accurately reproduce the measured reflectance spectra. The substrates RO3010 and RT/duroid 6010.2LM exhibit significant frequency dispersion of both their relative permittivity and loss tangent. Conversely, the thermoset microwave laminate TMM10i is characterized by both a lower frequency dispersion and overall dielectric losses, thus making it a promising candidate for the design of low-profile and broadband components for novel terahertz applications. Owing to the simple Lorentzian dispersion model used for the description of the relative permittivity, the presented results can serve as a reference, and they can be directly introduced in design and optimization workflows for novel devices in emerging terahertz applications.

Keywords: high-permittivity substrates; Rogers laminates; terahertz time-domain spectroscopy; dielectric material characterization; dielectric dispersion

Citation: Fuscaldo, W.; Maita, F.; Maiolo, L.; Beccherelli, R.; Zografopoulos, D.C. Broadband Dielectric Characterization of High-Permittivity Rogers Substrates via Terahertz Time-Domain Spectroscopy in Reflection Mode. *Appl. Sci.* **2022**, *12*, 8259. https://doi.org/10.3390/app12168259

Academic Editor: Wei Hu

Received: 28 June 2022
Accepted: 15 August 2022
Published: 18 August 2022

1. Introduction

At microwave and millimeter-wave frequencies, printed circuit board (PCB) technology is extensively used for its versatility, the commercial availability of the employed materials, and the relatively low-cost and simple fabrication process in the design of planar waveguiding and radiating devices, e.g., filters, polarizers, and antennas [1].

Although there exist a large variety of laminates, those commonly employed in PCB technology consist of ceramics, polytetrafluoroethylene (PTFE), and epoxy resin composites sometimes reinforced with glass fibers to gain in stability. The dielectric properties of these materials may vary a lot from one type to another (for instance, FR-4 are usually lossier and cheaper than Rogers substrates [2]), but they almost all exhibit relatively low frequency dispersion of both the relative permittivity and the loss tangent, which are usually provided by the manufacturer at 1 GHz and/or 10 GHz. Thus, the dielectric characterization at these frequencies can be safely interpolated over a relatively large frequency range with a constant fit.

However, the ever-increasing needs for high data rates and lower latencies [3–5] required by modern applications, such as next-generation wireless communications, call for components featuring bandwidths in the order of tens of GHz that are not available in the current 5G band allocations [5,6]. Therefore, these needs require a shift in the usage of the frequency spectrum, from the more conventional microwave domain to the millimeter-wave and sub-terahertz (THz) frequency range where IEEE has recently released a standard for mobile communications, namely the IEEE standard 802.15.3d-2017 [7].

At such high frequencies, the dielectric properties of widely employed PCB materials can significantly change from those provided by the manufacturer at lower frequencies, thus calling for an accurate characterization, which is also capable of dealing with the possible non-negligible frequency dispersion of the generally complex-valued dielectric constant. This aspect is of key importance for the design of future components, whose performance can be dramatically influenced by the frequency dispersion of both the dielectric permittivity and loss tangent.

That said, commercial laminates such as those from Rogers and Taconic are potential candidates for applications in millimeter-wave or (sub-)THz frequencies [8]. However, only few works [1,9–11] reported thus far a characterization of the dielectric properties of common laminates at millimeter-wave and/or sub-THz frequencies. In [1], Rogers and Taconic substrates were characterized in the W-band (namely, 75–110 GHz) through a voltage network analyzer (VNA) approach: the dielectric properties were extracted from the S-parameters of a substrate-integrated waveguide (SIW) resonator. In [11], Rogers substrates were characterized through THz time-domain spectroscopy (TDS) at higher frequencies (viz., 0.2–1.8 THz), whereas the works in [9,10] compared and complemented the THz-TDS measurements of low-temperature cofired ceramics [9] and Rogers substrates [10] with VNA measurements. Indeed, THz-TDS measurements cannot provide accurate results at frequencies below 300 GHz where there is not enough dynamic range with respect to the noise floor. Conversely, VNA measurements provide accurate results below 300 GHz but extensions are available only up to 1.5 THz (with a substantial increase of equipment cost). The two approaches, namely THz-TDS and VNA, can thus be seen as complementary, yet they produce comparable results [12].

Notwithstanding, most THz-TDS measurements are performed in transmission mode (see, e.g., [13]), and only in few cases the reflection mode [14–17] has been exploited; in none of these cases the properties of the Rogers materials have been characterized. However, as recently emphasized in [17], the reflection mode not only represents a powerful, effective technique for retrieving the complex-valued frequency dispersion of the dielectric properties of moderately reflective and lossy materials, but it also represents a natural environment (as opposed to the transmission mode) for backmetallized substrates. The latter represents a key component in systems such as THz antenna [18–20] and static or reconfigurable reflective metasurfaces for THz-wave manipulation, e.g., absorption [21,22] or beam steering [23].

For this purpose, we report here for the first time a THz-TDS characterization in reflection mode of three types of high-permittivity Rogers laminates (RO3010, RO/duroid 6010.2LM, and TMM10i), representative of different product series, in the sub-THz range (namely, from 0.3–1 THz). The frequency dispersion of their complex dielectric permittivity is described by a single standard Lorentzian term, which is shown to accurately reproduce the experimentally measured reflectance spectra through a fitting optimization procedure based on an analytical transmission-line model.

Despite the fact that all three materials have similar nominal properties in the microwave X-band, the study clearly demonstrates their different dielectric properties in the investigated sub-THz spectrum. It is shown that RO3010 and RO/duroid 6010.2LM exhibit significant frequency dispersion, which cannot be neglected in the design of broadband THz components. On the contrary, TMM10i is characterized by both a low frequency dispersion and overall lower dielectric losses. Combined with its high permittivity, which allows for denser circuit integration and/or lower thickness profile, these results highlight the potential of thermoset laminates (such as TMM10i) for the design of novel devices for emerging THz applications. Thanks to its simplicity, the retrieved Lorentz frequency dispersion of the complex permittivity for the three materials can provide a benchmark reference and it can be directly embedded in component design processes involving (semi-)analytical, frequency- or time-domain methods.

2. Terahertz Time-Domain Spectroscopy of High-Permittivity Substrates

2.1. Materials

The materials characterized in this work are three of the most popular high-permittivity microwave substrates, made commercially available by Rogers Corporation: RO3010™, RT/duroid 6010.2LM™, and TMM10i™ [24]. The first two are ceramic-filled PTFE composites for use in commercial microwave and RF applications. RO3010 exhibits negligible permittivity dispersion up to 50 GHz and an almost copper-matched coefficient of thermal expansion (CTE). The third one is a thermoset microwave laminate with low thermal coefficient and low frequency dispersion of dielectric permittivity (in the microwave range), copper-matched CTE, and high thermal conductivity facilitating heat dissipation and removal.

Table 1 summarizes the main material and dielectric properties of the three investigated samples. It is stressed that in all cases, the values of their relative permittivity ε'_r and loss tangent $\tan\delta$ ($\varepsilon_r := \varepsilon'_r(1 - j\tan\delta)$ being the complex-valued relative permittivity), as provided by the manufacturer at 10 GHz, are very similar: $\varepsilon'_r \simeq 10$ and $\tan\delta \simeq 0.002$. However, it has been shown in scarcely available literature data that the dielectric properties of standard microwave substrates can significantly differ in the sub-THz spectral range [10,11]. Moreover, the dielectric permittivity and loss tangent values are usually extracted by inversion algorithms that produce a discrete set of frequency-dependent values that do not necessarily satisfy the Kramers–Kronig relations, essential to preserve causality in the frequency-domain dielectric function [25]. In this work, we investigated the dispersion of the complex permittivity of the three benchmark materials via THz-TDS by accurately fitting to a single-term Lorentzian model [25], which provided a readily available analytic and consistent expression to be used both in frequency- and time-domain simulations, such as the broadly used finite-difference time-domain method [26,27].

Table 1. Properties of the investigated high-permittivity substrates. Relative dielectric constant and loss tangent values were provided by Rogers Corporation at 10 GHz.

Name	Composition	Thickness (mm)	ε'_r	tanδ
RO3010	Ceramic-filled PTFE composites	1.270 ± 0.051	10.2 ± 0.25	0.0022
RT/duroid 6010.2LM	Ceramic-filled PTFE composites	1.905 ± 0.102	10.2 ± 0.25	0.0023
TMM10i	Ceramic, hydrocarbon, thermoset polymer composites	1.270 ± 0.038	9.8 ± 0.245	0.002

2.2. Methods

First, the samples were prepared for the measurement by etching the 35 µm electrodeposited copper film from one side of the substrates. This was done by depositing a 15 µm thick resin FP415 by ElgaEurope using a low temperature (120 °C) lamination technique (Bungard RLM 419P) as a protection layer. Then, the exposed copper side was etched by immersing the samples in a copper wet etching solution (100 mL H_2O, 60 ml HCL, 20 mL H_2O_2) at 25 °C for 4 min. A dry resin stripper was then applied for 3 min to remove the resist and finally the sample was rinsed in isopropanol and deionized water.

The processed Rogers substrates with a bare top side and a backmetallized side were investigated in reflection mode using TeraFlash Pro [28], a THz-TDS instrument which allows the broadband characterization of the samples in the sub-THz range. The measurement procedure has been recently presented in detail [17] and its main aspects are briefly reported next for the readers' convenience. The schematic of the employed standard reflection-mode configuration of the THz-TDS setup is shown in Figure 1a. The laser source of the instrument is the FemtoFErb THz FD6.5 laser, which generates 50 fs pulses at 1560 µm with a repetition rate of 100 MHz [28]; optical fibers bring these laser pulses to the emitter, which radiates an electromagnetic THz signal through a photoconductive antenna. The terahertz wave impinges on the sample at a fixed oblique angle of $\theta_i = 8°$. A photo of

the THz wave propagation module of the setup with a sample placed for measurement is shown in Figure 1b. In all cases, we averaged 100 pulses for each time-domain pulse trace $s(t)$ over a 200 ps time window (see Figure 2a) to obtain a spectral resolution of 10 GHz. We then analyzed the frequency-domain reflection spectra over the range 0.3–1 THz (see Figure 2b), which ensures more than 80 dB of dynamic range with respect to the noise floor.

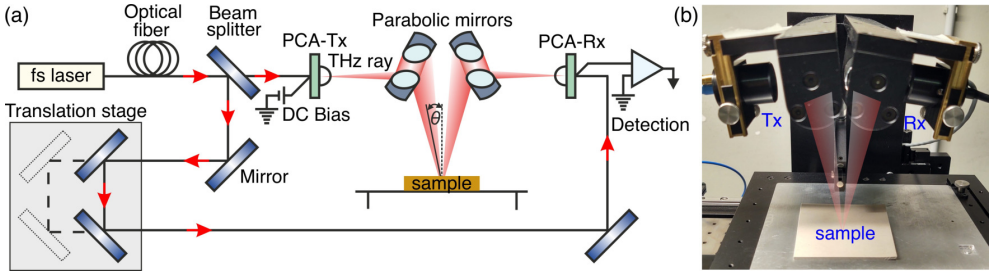

Figure 1. (**a**) Schematic of the employed THz-TDS setup, configured for sample characterization in reflection mode. The setup consists of an fs-pulse, near-infrared laser, photoconductive transmit (Tx) and receive (Rx) antennas, an optical delay line, a set of mirrors, and the sample under test placed on a metallic baseplate. The optical beam path is marked with red arrows and the THz wave path by red-shaded elements. (**b**) Photo showing the THz-wave propagation module of the TDS setup with a sample placed on the metallic baseplate.

We started from a preliminary analysis of the signal in the time domain. Here, we estimated the thickness of the substrates from the arrival times of the zeroth-order echo (reflection from the top side of the substrate) with the formula provided in ([17], [Equation (1)]). Results were consistent with the nominal thickness values and their tolerance, as provided by the manufacturer and summarized in Table 1.

However, we were interested in an accurate material characterization of the substrates, which took into account the losses and frequency dispersion. To this aim, in analogy with the procedure carried out in [17], we developed an equivalent circuit model (see Figure 3) to derive a theoretical amplitude reflection coefficient R_{th} (a time dependence $\exp(j\omega t)$ of the fields was assumed) at the air–substrate interface, viz., $z = 0$. Thus, by definition (see, e.g., [29]) we had $R_{\mathrm{th}} = |Y_{\mathrm{c}} - Y_{\mathrm{in}}|/|Y_{\mathrm{c}} - Y_{\mathrm{in}}|$, where Y_{c} and Y_{in} are the characteristic admittance at $z = 0^{+}$ and the input admittance looking downwards at $z = 0^{-}$, respectively. According to Figure 2b, $Y_{\mathrm{c}} = Y_0$, Y_0 is the wave admittance in the air, and $Y_{\mathrm{in}} = -jY_{\varepsilon}\cot(k_{z\varepsilon}d)$, Y_{ε} and $k_{z\varepsilon}$ are the wave admittance and the propagating wavenumber in the dielectric substrate of thickness d. The amplitude reflection coefficient finally reads:

$$R_{\mathrm{th}} = \left| \frac{\cos\theta_{\mathrm{i}} - j\sqrt{\varepsilon_{\mathrm{r}} - \sin^2\theta_{\mathrm{i}}}\cot\left(k_0 d\sqrt{\varepsilon_{\mathrm{r}} - \sin^2\theta_{\mathrm{i}}}\right)}{\cos\theta_{\mathrm{i}} + j\sqrt{\varepsilon_{\mathrm{r}} - \sin^2\theta_{\mathrm{i}}}\cot\left(k_0 d\sqrt{\varepsilon_{\mathrm{r}} - \sin^2\theta_{\mathrm{i}}}\right)} \right| \tag{1}$$

where k_0 is the vacuum wavenumber.

R_{th} was then compared with that of the measured amplitude reflection coefficient R_{meas}, which was obtained from the frequency-domain measurements as the ratio between the amplitude of the reflection spectrum $|S(f)|$ from the substrate over the reference measurement in its absence. Figure 2b shows a couple of indicative power spectra $|S(f)|^2$, reference and sample, measured for the substrate RO3010. For the calculation of R_{th}, we considered that the substrate relative permittivity was described by a standard single-term Lorentz model [25]:

$$\varepsilon_{\mathrm{r}}(f) = \varepsilon_{\infty} + \frac{(\varepsilon_{\mathrm{s}} - \varepsilon_{\infty})f_0^2}{f_0^2 - f^2 + j\frac{f}{2\pi\tau}} \tag{2}$$

where ε_s, ε_∞ are the relative permittivity values at DC and infinite frequency, respectively, and f_0 and τ are the Lorentz resonant frequency and decay time, respectively. These four parameters were introduced as free variables in a standard optimization process based on the Nelder–Mead simplex method implemented in MATLAB©, which minimized the ℓ^2-norm of the difference $R_{th} - R_{meas}$ over the 0.3–1 THz spectral window of investigation. In other words, the four-dimensional (4D) optimization problem consisted in seeking the optimum values of ε_s, ε_∞, f_0, τ such that:

$$\min_{\{\varepsilon_s, \varepsilon_\infty, f_0, \tau\}} \left(\sqrt{\int_{f_{min}}^{f_{max}} |R_{th} - R_{meas}|^2 df} \right) \quad (3)$$

where $f_{min} = 0.3$ THz and $f_{max} = 1$ THz. This minimization process provided a 4-tuple of optimum values to be applied into (2) to get the best fit of R_{meas}. In Section 2.3, these values are provided for all Rogers substrates analyzed here, namely the RO3010, the 6010.2LM and the TMM10i.

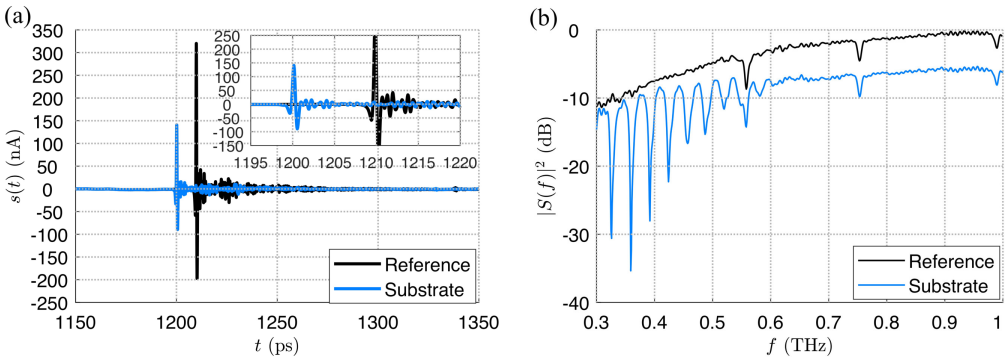

Figure 2. (**a**) Time-domain signal $s(t)$ measured for the reference (reflection from the metallic baseplate) and in the presence of the RO3010 substrate. The pulse around 1200 ps (light blue curve) preceding the reference one stems from reflection from the top surface of the substrate. A zoomed inset is reported at the top-right corner to better show the shape of the pulses. (**b**) Fourier transformed power spectra of the time-domain signals. The three major dips in the reference spectrum are due to water absorption.

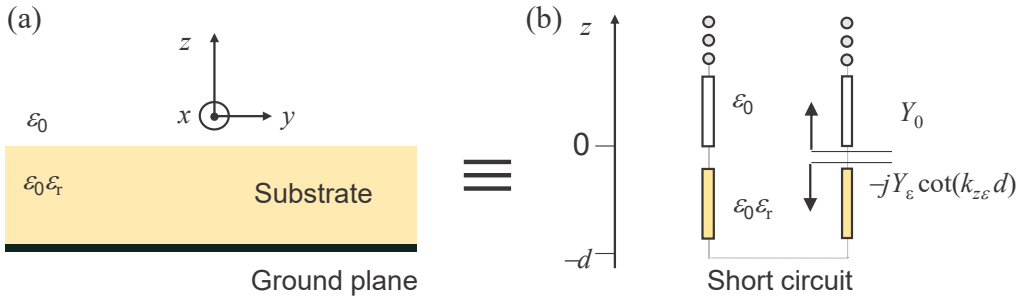

Figure 3. (**a**) One-dimensional section of the backmetallized substrate under test and (**b**) its transmission-line equivalent model.

2.3. Results

The methodology described in the previous subsection was applied to the dielectric characterization of the three investigated Rogers substrates. The obtained results are summarized in Figure 4, where the first two columns report the relative permittivity and loss tangent frequency dispersion, as per the optimized fit to the Lorentz model, and the third column shows a comparison between the measured and theoretical fit of the power reflectance coefficients $|R_{meas}|^2$ and $|R_{th}|^2$. The Lorentz parameters for the three materials are summarized in Table 2. We highlight here that the dispersion model in this study is phenomenological, aiming to accurately describe the dielectric frequency dispersion of the

three investigated materials with a minimum number of terms so as to facilitate its use in the design flow of THz components.

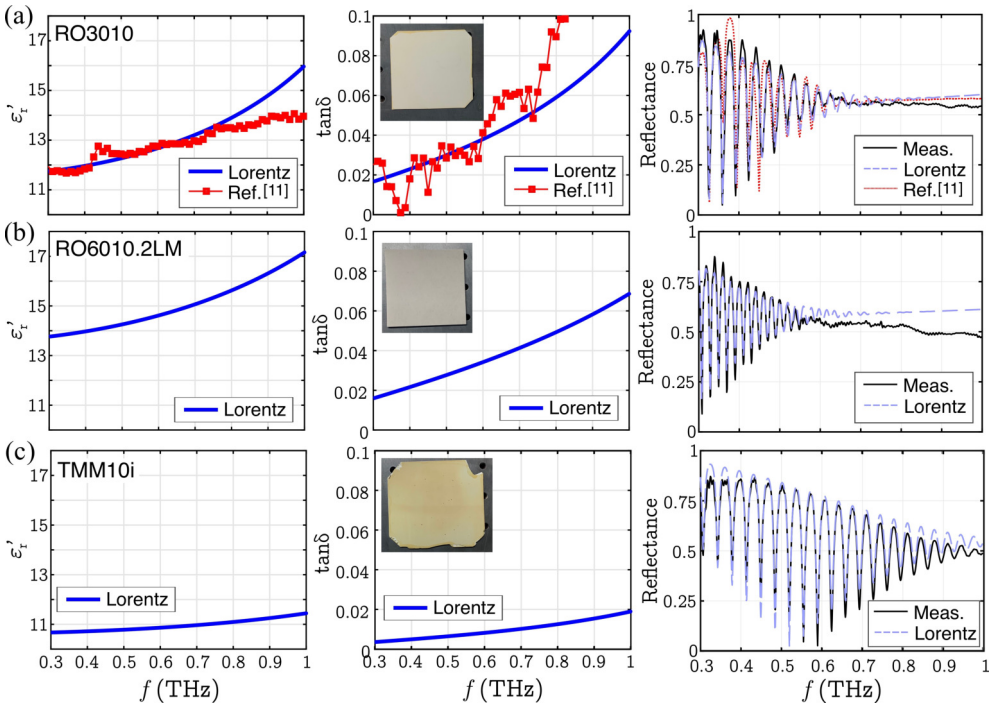

Figure 4. Relative dielectric permittivity, loss tangent, and comparison between measured and simulated spectra based on the Lorentz-fitted permittivities of the three investigated substrates: (**a**) RO3010, (**b**) RT/duroid 6010.2LM, and (**c**) TMM10i. The insets in the second column show photos of the characterized samples with an area of approximately 5×5 cm^2. In (**a**), results are compared to the data provided in [11].

Table 2. Lorentz model parameters calculated for the investigated Rogers high-permittivity substrates.

Name	ε_∞	ε_s	f_0 (THz)	τ (ps)
RO3010	3.223	11.464	1.663	0.779
RT/duroid 6010.2LM	1.001	13.502	2.083	0.654
TMM10i	7.923	10.611	2.008	0.424

In the case of RO3010 in Figure 4a, we also included the tabulated data for the measurements reported in [11], showing good overall agreement. We note that the simulated reflectance spectra based on the reference data do not accurately reproduce our measurements, as shown in the right panel of Figure 4a. A comparison of the complex relative permittivity data for RO/duroid 6010.2LM is also in line with available literature information [10].

In the reflectance spectra one can notice an oscillating part with a diminishing amplitude towards the higher frequencies. This effect stems from the Fabry–Perot (FP) multiple reflections of the THz wave that enters and propagates in the substrate. The periodicity of these oscillations, also known as free spectral range (FSR) [30], can be estimated at a first approximation by the following formula:

$$\mathrm{FSR} = \frac{c_0}{2d\cos\theta_\mathrm{i}\sqrt{\varepsilon_\mathrm{r}'}} \tag{4}$$

The position of the FP maxima/minima depends directly on the thickness and relative permittivity, whereas the modulation depth depends on the loss tangent of the substrate.

Thus, the oscillating spectrum contains the necessary information for the dispersion model fitting. At higher frequencies the reflectance converges towards a constant value, which corresponds to the part of the THz wave that is reflected from the top surface of the substrate and depends also on its relative permittivity. It can be noticed that the measured high-frequency reflectance is a bit lower than the theoretical prediction. This is attributed to defocusing effects due to the substrate thickness, and considering its high permittivity and operation in reflection mode, which doubles the wave path distance. Indeed, the effect is more noticeable in the case of RO6010.2LM, which is thicker than the other two samples studied. Nevertheless, in the investigated examples the important information in the reflection spectra is contained in the lower-frequency part, which is very well reproduced by the theoretical model, so relevant correction techniques were not applied [31].

The results revealed different trends for the three materials, despite the fact that their dielectric properties were almost identical at the microwave frequency of 10 GHz, as summarized in Table 1. RO3010 and RO/duroid 6010.2LM show a significant frequency dispersion with their relative permittivity (loss tangent) approximately in the range of 12–16 (0.02–0.1) and 14–17 (0.02–0.07), respectively, in the investigated spectral window. Such a level of frequency dispersion needs to be taken into account in the design of components as it might significantly impact their performance. On the contrary, the thermoset laminate TMM10i shows a significantly lower frequency dispersion ($10.7 \leq \varepsilon_r \leq 11.4$) and lower values of loss tangent ($0.008 \leq \tan\delta \leq 0.03$), both highly desirable properties for high-performance and broadband devices. Overall, the retrieved Lorentz dispersion models accurately reproduce the measurements and constitute a reference for the engineering of novel, low-profile components in emerging applications in the sub-THz spectrum.

3. Conclusions

To sum up, we characterized three popular high-permittivity substrates (RO3010, RO/duroid 6010.2LM, and TMM10i), commercially available from Rogers Corporation, in the sub-THz range based on THz-TDS measurements in reflection mode. It was shown that by fitting the complex relative permittivity of the substrates to a single Lorentzian term, the theoretically calculated reflection spectra accurately matched the measurements. The substrates RO3010 and RT/duroid 6010.2LM showed a significant dispersion in the investigated frequency range, which has to be taken into account in THz component design. In comparison, the substrate TMM10i showed both a lower dispersion and significantly lower loss tangent, both highly desirable properties. Thanks to the standard Lorentzian dispersion model used for their fitting, the presented reference data can be directly incorporated in design and optimization workflows of devices for emerging THz applications, including time-domain simulation methods or semianalytical algorithms.

Author Contributions: Conceptualization, W.F. and D.C.Z.; methodology, W.F. and D.C.Z.; measurements, W.F., F.M., L.M. and D.C.Z.; software, W.F.; data processing, W.F. and D.C.Z.; writing—original draft preparation, D.C.Z.; writing—review and editing, all authors; supervision, R.B. and D.C.Z. All authors have read and agreed to the published version of the manuscript.

Funding: This research received no external funding.

Data Availability Statement: The data presented in this study are available from the corresponding author upon reasonable request.

Acknowledgments: We would like to thank Stefano Dadà and Rogers Corporation for providing us with the substrates investigated in this work.

Conflicts of Interest: The authors declare no conflict of interest.

References

1. Cheng, Y.J.; Liu, X.L. W-band characterizations of printed circuit board based on substrate integrated waveguide multi-resonator method. *IEEE Trans. Microw. Theory Tech.* **2016**, *64*, 599–606. [CrossRef]
2. Al-Yasir, Y.I.; Alkhafaji, M.K.; Alhamadani, H.A.; Ojaroudi Parchin, N.; Elfergani, I.; Saleh, A.L.; Rodriguez, J.; Abd-Alhameed, R.A. A new and compact wide-band microstrip filter-antenna design for 2.4 GHz ISM band and 4G applications. *Electronics* **2020**, *9*, 1084. [CrossRef]
3. Nagatsuma, T.; Ducournau, G.; Renaud, C.C. Advances in terahertz communications accelerated by photonics. *Nat. Photon.* **2016**, *10*, 371–379. [CrossRef]
4. Pirrone, D.; Ferraro, A.; Zografopoulos, D.C.; Fuscaldo, W.; Szriftgiserand, P.; Ducournau, G.; Beccherelli, R. Metasurface-based Filters for High Data Rate THz Wireless Communications: Experimental Validation of a 14 Gbps OOK and 104 Gbps QAM-16 Wireless Link in the 300 GHz band. *IEEE Trans. Wirel. Commun.* **2022** . [CrossRef]
5. Rappaport, T.S.; Xing, Y.; Kanhere, O.; Ju, S.; Madanayake, A.; Mandal, S.; Alkhateeb, A.; Trichopoulos, G.C. Wireless Communications and Applications Above 100 GHz: Opportunities and Challenges for 6G and Beyond. *IEEE Access* **2019**, *7*, 78729–78757. [CrossRef]
6. Xing, Y.; Rappaport, T.S. Terahertz wireless communications: Co-sharing for terrestrial and satellite systems above 100 GHz. *IEEE Commun. Lett.* **2021**, *25*, 3156–3160. [CrossRef]
7. *IEEE Standard for High Data Rate Wireless Multi-Media Networks–Amendment 2: 100 Gb/s Wireless Switched Point-to-Point Physical Layer in IEEE Std 802.15.3d-2017, (Amendment to IEEE Std 802.15.3-2016 as amended by IEEE Std 802.15.3e-2017)*; IEEE: Piscataway, NJ, USA , 2017; pp. 1–55.
8. Zhu, H.T.; Liu, D.; Hu, J.; Li, S.; Shi, S.C.; Xue, Q.; Che, W. Low-Loss, Thermally Insulating, and Flexible Rectangular Dielectric Waveguide for Sub-THz—Signal Coupling in Superconducting Receivers. *IEEE Trans. Terahertz Sci. Technol.* **2020**, *10*, 190–199. [CrossRef]
9. Ma, M.; Wang, Y.; Navarro-Cia, M.; Liu, F.; Zhang, F.; Liu, Z.; Li, Y.; Hanham, S.M.; Hao, Z. The dielectric properties of some ceramic substrate materials at terahertz frequencies. *J. Eur. Ceram. Soc.* **2019**, *39*, 4424–4428. [CrossRef]
10. Ruan, X.; Chan, C.H. Terahertz free-space dielectric property measurements using time- and frequency-domain setups. *Int. J. RF Microw. Comput.-Aided Eng.* **2019**, *29*, e21839. [CrossRef]
11. Hejase, J.A.; Paladhi, P.R.; Chahal, P.P. Terahertz Characterization of Dielectric Substrates for Component Design and Nondestructive Evaluation of Packages. *IEEE Trans. Compon. Packag. Manuf. Technol.* **2011**, *1*, 1685–1694. [CrossRef]
12. Naftaly, M.; Vieweg, N.; Deninger, A. Industrial applications of terahertz sensing: State of play. *Sensors* **2019**, *19*, 4203. [CrossRef] [PubMed]
13. Withayachumnankul, W.; Naftaly, M. Fundamentals of Measurement in Terahertz Time-Domain Spectroscopy. *J. Infrared Millim. Terahertz Waves* **2013**, *35*, 610–637. [CrossRef]
14. Jepsen, P.U.; Jensen, J.K.; Møller, U. Characterization of aqueous alcohol solutions in bottles with THz reflection spectroscopy. *Opt. Express* **2008**, *16*, 9318. [CrossRef] [PubMed]
15. Mackenzie, D.M.A.; Whelan, P.R.; Bøggild, P.; Jepsen, P.U.; Redo-Sanchez, A.; Etayo, D.; Fabricius, N.; Petersen, D.H. Quality assessment of terahertz time-domain spectroscopy transmission and reflection modes for graphene conductivity mapping. *Opt. Express* **2018**, *26*, 9220. [CrossRef] [PubMed]
16. Ahi, K.; Shahbazmohamadi, S.; Asadizanjani, N. Quality control and authentication of packaged integrated circuits using enhanced-spatial-resolution terahertz time-domain spectroscopy and imaging. *Opt. Lasers Eng.* **2018**, *104*, 274–284. [CrossRef]
17. Fuscaldo, W.; Simone, S.D.; Dimitrov, D.; Marinova, V.; Mussi, V.; Beccherelli, R.; Zografopoulos, D.C. Terahertz characterization of graphene conductivity via time-domain reflection spectroscopy on metal-backed dielectric substrates. *J. Phys. D Appl. Phys.* **2022**, *55*, 365101. [CrossRef]
18. Fuscaldo, W.; Tofani, S.; Zografopoulos, D.C.; Baccarelli, P.; Burghignoli, P.; Beccherelli, R.; Galli, A. Systematic Design of THz Leaky-Wave Antennas based on Homogenized Metasurfaces. *IEEE Trans. Antennas Propag.* **2018**, *66*, 1169–1178. [CrossRef]
19. Fuscaldo, W.; Burghignoli, P.; Baccarelli, P.; Galli, A. Graphene Fabry-Perot Cavity Leaky-Wave Antennas: Plasmonic Versus Nonplasmonic Solutions. *IEEE Trans. Antennas Propag.* **2017**, *65*, 1651–1660. [CrossRef]
20. Fuscaldo, W.; Burghignoli, P.; Galli, A. The Transition Between Reactive and Radiative Regimes for Leaky Modes in Planar Waveguides Based on Homogenized Partially Reflecting Surfaces. *IEEE Trans. Microw. Theory Tech.* **2020**, *68*, 5259–5269. [CrossRef]
21. Isić, G.; Vasić, B.; Zografopoulos, D.C.; Beccherelli, R.; Gajić, R. Electrically Tunable Critically Coupled Terahertz Metamaterial Absorber Based on Nematic Liquid Crystals. *Phys. Rev. Appl.* **2015**, *3*, 064007. [CrossRef]
22. Astorino, M.D.; Fastampa, R.; Frezza, F.; Maiolo, L.; Marrani, M.; Missori, M.; Muzi, M.; Tedeschi, N.; Veroli, A. Polarization-maintaining reflection-mode THz time-domain spectroscopy of a polyimide based ultra-thin narrow-band metamaterial absorber. *Sci. Rep.* **2018**, *8*, 1985. [CrossRef] [PubMed]
23. Vasic, B.; Isic, G.; Beccherelli, R.; Zografopoulos, D.C. Tunable Beam Steering at Terahertz Frequencies Using Reconfigurable Metasurfaces Coupled With Liquid Crystals. *IEEE J. Sel. Top. Quantum Electron.* **2020**, *26*, 1–9. [CrossRef]
24. Rogers Corporation. Advanced Electronic Solutions, RF Solutions Laminates and 3D Printable Materials. Available online: https://rogerscorp.com/advanced-electronics-solutions (accessed on 17 June 2022).
25. Balanis, C.A. *Advanced Engineering Electromagnetics*; Wiley Online Library: Hoboken, NJ, USA, 2012; Volume 111.

26. Zografopoulos, D.C.; Prokopidis, K.P.; Dąbrowski, R.; Beccherelli, R. Time-domain modeling of dispersive and lossy liquid-crystals for terahertz applications. *Opt. Mater. Express* **2014**, *4*, 449. [CrossRef]
27. Prokopidis, K.P.; Zografopoulos, D.C. Time-Domain Studies of General Dispersive Anisotropic Media by the Complex-Conjugate Pole–Residue Pairs Model. *Appl. Sci.* **2021**, *11*, 3844. [CrossRef]
28. TOPTICA Photonics AG. TeraFlash Pro, Versatile Time-Domain Terahertz Platform. Available online: https://www.toptica.com/products/terahertz-systems/time-domain/teraflash-pro (accessed on 19 June 2022).
29. Pozar, D.M. *Microwave Engineering*; John Wiley & Sons: Hoboken, NJ, USA, 2009.
30. Burghignoli, P.; Fuscaldo, W.; Galli, A. Fabry–Perot Cavity Antennas: The Leaky-Wave Perspective [Electromagnetic Perspectives]. *IEEE Antennas Propag. Mag.* **2021**, *63*, 116–145. https://doi.org./10.1109/MAP.2021.3085199. [CrossRef]
31. Mrnka, M.; Appleby, R.; Saenz, E. Accurate S-Parameter Modeling and Material Characterization in Quasi-Optical Systems. *IEEE Trans. Terahertz Sci. Technol.* **2022**, *12*, 199–210. [CrossRef]